ChemComm

Accepted Manuscript

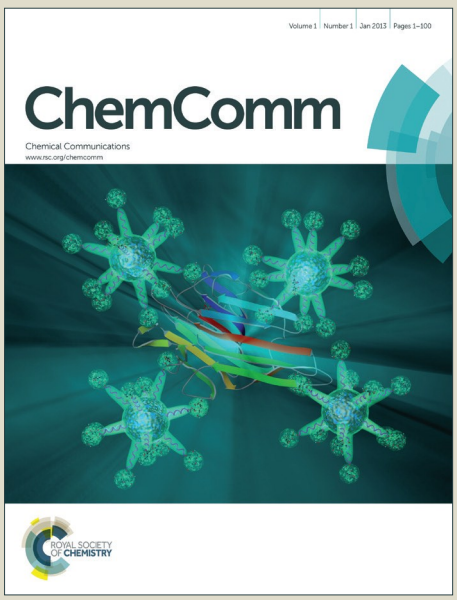

ROYAL SOCIETY OF CHEMISTRY

www.rsc.org/chemcomm

Cite this: DOI: 10.1039/c0xx00000x

www.rsc.org/xxxxxx

ARTICLE TYPE

Improved electrochemical performance of CoS_2/MWCNT nanocomposites for sodium-ion batteries

Zulipiya Shadike[ab] ,Ming-Hui Cao[a], Fei Ding[b], Lin Sang[b], Zheng-Wen Fu[a*]

Received (in XXX, XXX) XthXXXXXXXXX 20XX, Accepted Xth XXXXXXXXX 20XX

DOI:

A CoS_2/multi-walled carbon nanotube (MWCNT) nanocomposite was synthesized and its sodium storage performances in ether-based electrolyte and commonly used carbonate-based electrolyte were investigated for the first time. A high capacity of 568 mAh g^{-1} after 100 cycles in ether-based electrolyte can be achieved.

Sodium ion batteries (SIBs) have recently gained recognition as an intriguing candidate for next-generation battery systems instead of lithium ion batteries (LIBs) [1-3]. As a class of remarkable sodium storage materials with high capacity for SIBs, considerable efforts have been devoted to investigating the electrochemical properties of various metal sulfides such as TiS_2[4], SnS[5], Cu_2S [6], Ni_3S_2[7], MoS_2[8], WS_2[9] and FeS_2[10-12]. The conversion-cum-alloy based anode material SnS was firstly reported by Dutta et al[5]. Such a nanostructured electrode showed reversible capacity of 325 mAh g^{-1} after 30 cycles at 125 mA g^{-1}. Kim et al. reported the sodium storage performance and electrochemical reaction mechanism of Cu_2S[6]. The results indicated that Cu_2S electrode exhibits an initial capacity of 294 mAh g^{-1} followed by formation of Na_xCu_2S (x<2), and decreases to 261 mAh g^{-1} after 20 cycles. The comparisons of the electrochemical performances of Ni_3S_2 in different electrolytes were also reported by Kim et al[7]. Among the electrolytes, TEGDME with $NaCF_3SO_3$ showed the lowest interfacial resistance and good capacity retention (250 mAh g^{-1} after 40 cycles). Furthermore, the carbonaceous support materials were developed for improving cyclic performance of electrodes. For example, Wang et. al. reported exfoliated MoS_2–C composite with outstanding electrochemical performance[8], in which MoS_2-C electrode could maintain an almost stable capacity of 390 mAh g^{-1} over 100 cycles. Likewise, Su et al. demonstrated that WS_2/graphene nanocomposites exhibit a high reversible capacity of about 590 mAh g^{-1} and still retain 329 mAh g^{-1}capacity after 100 cycles[9]. Recently studies indicated that the cyclability of FeS_2 can be improved by using an ether-based electrolyte (1.0 M $NaCF_3SO_3$ in diglyme) instead of the commonly used carbonate-based electrolyte, in which FeS_2 electrode could deliver a high sodiation capacity of 530 $mAhg^{-1}$ and retain 450 $mAhg^{-1}$ after 100 cycles[11], and 170 $mAhg^{-1}$ can be achieved after 20000 cycles[12]. These works provided rich information on sodium electrochemistry of metal sulfides and the possibility of using them as storage energy materials for the application and development of rechargeable SIBs. Here, an attempt to extend the investigation of electrochemical properties of other metal sulfides such as cobalt sulfides was made.

Cobalt sulfide is an interesting metal chalcogenide semiconductor material and has a number of applications in dye-sensitized solar cells[13-15], supercapacitors[16-18], and lithium ion batteries[19-25]. Recently, superior Li-storage properties of cobalt sulfide could be achieved by designing special structured materials and fabricating nanocomposites with carbon materials (such as carbon coated materials, graphene hybrid nanocomposites). To our knowledge, there is no available report on the sodium electrochemistry of cobalt sulfides.

Here, we firstly report sodium storage properties of CoS_2 materials synthesized by a simple hydrothermal method and compare their electrochemical performances in ether-based electrolyte and commonly used carbonate-based electrolyte. Integration of metal sulfides with carbon nanotubes (CNTs) is expected to be effective for enhancing the cyclability of CoS_2 electrode in SIBs like as previously reported graphene and other carbonaceous support materials. The morphology changes and the electrochemical performances of both CoS_2 and CoS_2/multi-walled carbon nanotube (MWCNT) electrodes during discharge/charge processes will be investigated. The motivation of this work is to explore the possibility of using cobalt sulfides as Na-storage material for SIBs and to elucidate its electrochemical reaction mechanism with sodium.

The structures of samples are investigated by XRD and Raman spectroscopy. Fig. 1(a) shows XRD patterns of the as-synthesized CoS_2 and CoS_2/MWCNT composites. The dominant diffraction peaks of both samples correspond to CoS_2, which can be indexed to the standard cubic phase of CoS_2 (JCPDS Card No. 41-1471). This result indicates that the bare CoS_2 and CoS_2/MWCNT composites are successfully synthesized without other polysulfide by a simply hydrothermal process. The structural features of synthesized CoS_2 and CoS_2/MWCNT samples are examined using Raman spectrum as shown in Fig.1 (b). The datum of MWCNT is included for comparison. There are two Raman bands at 1600 cm^{-1} (G band) and 1339 cm^{-1} (D band) for the MWCNT. Two weak peaks at about 380 cm^{-1} and 426 cm^{-1} can be observed from the Raman spectrum of CoS_2, this is in close agreement with the data of CoS_2 single crystal[26]. As for the CoS_2/MWCNT nanocomposites, it is clearly seen that four peaks at 380, 426, 1339 and 1600 cm^{-1} could correspond to the characteristic peaks

[a]*Shanghai Key Laboratory of Molecular Catalysts and Innovative Materials, Department of Chemistry & Laser Chemistry Institute, Fudan University, Shanghai 200433, P.R. China*

[b]*National Key Laboratory of Science and Technology on Power Sources, Tianjin Institute of Power Sources, Tianjin 300384, P. R. China*

of CoS_2 and the D, G bands of MWCNT, respectively. The Thermo-gravimetric results of MWCNT and CoS_2/MWCNT composite (Figure S1) indicate a 12% of MWCNT in the composite. The morphologies and composites of as-prepared

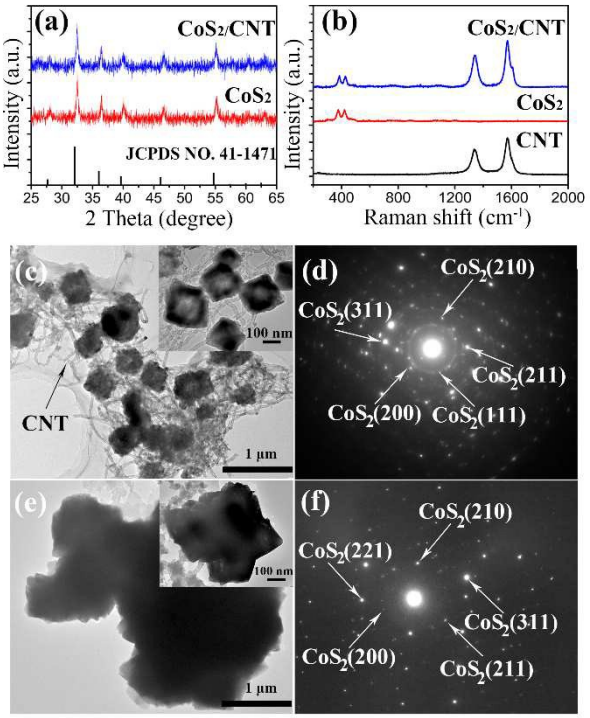

Figure.1 (a) XRD patterns of as synthesized CoS_2 and CoS_2/MWCNT;(b) Raman spectra of MWCNT, CoS_2 and CoS_2/MWCNT; TEM images and corresponding SAED patterns of initial electrodes: (c, d) CoS_2/MWCNT and (e, f) CoS_2.

materials are further investigated by TEM and SAED and as shown in Fig. 1(c-f). Obviously, CoS_2 particles with average size of 150-200 nm are anchoring uniformly on the MWCNT (Fig. 1(c)), while the CoS_2 nanoparticles prepared without MWCNT (Fig. 1(e)) tend to agglomerate and grow into micron or sub-micron particles. Their corresponding SAED pattern of nanocomposites are shown in Fig.1 (d) and (f), respectively, the discrete diffraction spots can be unambiguously indexed to diffractions of bare cubic CoS_2 phase (JCPDS No. 41-1471). This is consistent with the XRD and Raman spectroscopy results.

Fig. 2(a) and (b) show the discharge/charge curves of CoS_2 and CoS_2/MWCNT electrodes in 1.0 M $NaCF_3SO_3$-DGM electrolyte at a current density of 100 mAg^{-1}, respectively. In the initial discharge process, CoS_2 electrode exhibits two obvious flat voltage plateaus at 1.4 and 1.1V. The first discharge curve of CoS_2/Na battery is similar to that of CoS_2/Li battery in the voltage ranges from 1.0 V to 2.9 V, in which two discharge voltage plateaus at 1.6 and 1.2 V in the first discharge process was observed[19], implying that the CoS_2/Na battery may hold a similar discharge reaction mechanism as CoS_2/Li battery. In the first cycle, the CoS_2 electrode delivers a high discharge capacity of 810 $mAhg^{-1}$ and charge capacity of 697 $mAhg^{-1}$ with a coulombic efficiency of 86%. The discharge/charge voltage profiles of CoS_2/MWCNT electrode (Fig. 2(b)) are very similar to those of CoS_2 electrode and the first discharge/charge capacities of CoS_2/MWCNT electrode are 826 and 770 mAh g^{-1} with its coulombic efficiency of 93% respectively. This result indicates that incorporating of MWCNT cannot change the electrochemical mechanism of the CoS_2 electrode. For the subsequent cycles, the discharge/charge curves of CoS_2 and CoS_2/MWCNT electrodes were almost overlapped, indicating that highly reversible process take place during the subsequent cycles. For the 2nd and 10th cycle, CoS_2 electrodes exhibit discharge capacities of 640 and 599 mAh g^{-1}, while the CoS_2/MWCNT electrodes still remains higher capacities of 735 and 704 mAh g^{-1}, respectively. These results demonstrate that CoS_2/MWCNT electrodes present larger capacity and better stability than those of bare CoS_2 electrodes. The same conclusion also can be made by using 1.0 M $NaClO_4$-EC/PC as an electrolyte. The electrochemical performance of both CoS_2 and CoS_2/MWCNT electrodes in 1.0 M $NaClO_4$-EC/PC electrolyte under the same current density are also tested and shown in Fig. S2 (a-b). In the initial cycle, the CoS_2 electrode displays a discharge capacity of 809 mAh g^{-1} and a charge capacity of 631 mAh g^{-1} with a low coulombic efficiency of 78%, and the values for CoS_2/MWCNT electrode are 815 and 722 mAh g^{-1}. In the subsequent cycles, the reversible discharge capacities of CoS_2 are 724 and 585 mAh g^{-1} for 2nd and 10th cycles and 735 and 701 mAh g^{-1} for the CoS_2/MWCNT electrode. For the comparison, the pure MWCNT electrodes in the same conditions are investigated. As shown in Fig. S3, the MWCNT electrodes display initial discharge capacity of 14 and 11 mAh g^{-1} in 1.0 M $NaCF_3SO_3$-DGM and 1.0 M $NaClO_4$-EC/PC. These results indicate that high discharge/charge capacity of CoS_2/MWCNT electrodes at voltage range of 1.0-2.9 V almost originate from the electrochemical reactions of CoS_2 with Na.

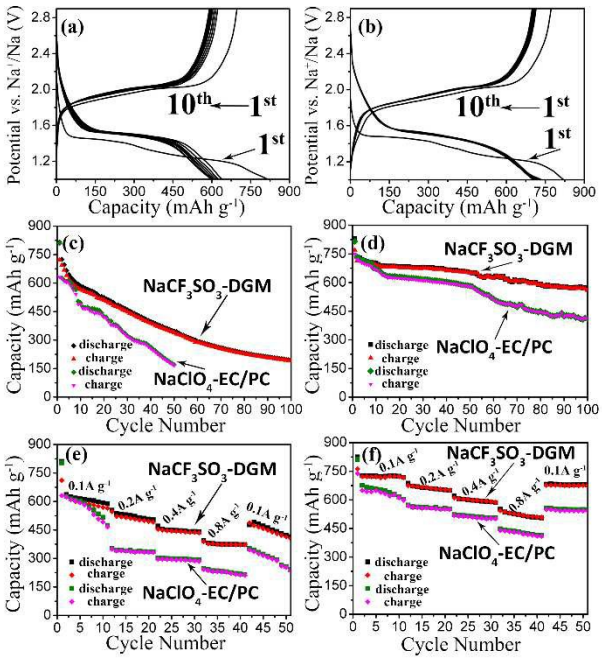

Figure.2 Discharge/charge curves of (a) CoS_2 and (b) CoS_2/MWCNT electrodes at a current density of 100 mA g^{-1}in 1 M $NaCF_3SO_3$-DGM; Cycle performance of (c) CoS_2 and (d) CoS_2/MWCNT electrodes at a current density of 100 mA g^{-1} in 1.0 M $NaCF_3SO_3$-DGM and 1.0 M $NaClO_4$-EC/PC; Comparison of rate capability between (e) CoS_2 and (f) CoS_2/MWCNT electrodes at various current densities in 1.0 M $NaCF_3SO_3$-DGM and 1.0 M $NaClO_4$-EC/PC.

Fig. 2(c-d) display the cycling performances of CoS_2 and CoS_2/MWCNT electrodes in ether and carbonate based electrolytes at current density of 100 mAh g^{-1}. As for CoS_2

electrode in $NaClO_4$-EC/PC shown in Fig. 2(c), the specific capacity rapidly drops to less than 170 mAh g^{-1} after 50 cycles and the capacity of CoS_2 electrode in $NaCF_3SO_3$-DGM decreases to 347 mAh g^{-1} after 50 cycles, which is 2 times than that of CoS_2 electrode in $NaClO_4$-EC/PC. However, after the 100 cycles, the CoS_2 electrode in $NaCF_3SO_3$- DGM shows the capacity of 190 mAh g^{-1}, which is 23.5% of the first discharge capacity. While CoS_2/MWCNT electrodes display surprisingly good cyclability with capacity retentions of 411 mAh g^{-1} after 100 cycles in $NaClO_4$-EC/PC (Fig. 2(d)), which is above 50% of the first discharge capacity. For CoS_2/MWCNT electrode in $NaCF_3SO_3$-DGM, the capacity maintains 568 mAh g^{-1} after 100 cycles (69% of first discharge capacity), which is significantly higher than of CoS_2/MWCNT electrode in $NaClO_4$-EC/PC and almost 3 times than that of CoS_2 electrode in the same conditions. As listed in table S1, the 100th discharge capacity of CoS_2/MWCNT electrode in $NaCF_3SO_3$-DGM is the highest in all metal-based electrodes reported previously. In addition, the CoS_2/MWCNT electrode possesses the highest energy density of 1027 Wh kg^{-1}, indicating that CoS_2/MWCNT can be considered as one of the most promising energy storage material for SIBs.

The outstanding cycling behaviors of CoS_2/MWCNT electrodes are also shown in the rate capability. As shown in Fig. 2(e), it can be seen that the CoS_2 electrode in $NaCF_3SO_3$-DGM displays discharge capacities of 636.4, 553.7, 470.5 and 393.6 mAh g^{-1} at the current densities of 0.1, 0.2, 0.4, and 0.8 A g^{-1}, respectively. For comparison, discharge capacities of the CoS_2 electrode in $NaClO_4$-EC/PC are found to be 626.1, 349.4, 296.2, and 242.3 mAh g^{-1} at the current densities of 0.1, 0.2, 0.4, and 0.8 A g^{-1}, respectively. It is clear that the rate performance of CoS_2 in $NaCF_3SO_3$-DGM is better than that of electrode in $NaClO_4$-EC/PC. In the same way, the CoS_2/MWCNT electrode in $NaCF_3SO_3$-DGM also shows well rate performance than that electrode in $NaClO_4$-EC/PC. As shown in Fig. 2(f), discharge capacities of the CoS_2/MWCNT in $NaCF_3SO_3$-DGM are about 726.6, 687,621 and 550.5 mAh g^{-1} at the current densities of 0.1, 0.2, 0.4, and 0.8 A g^{-1}, respectively. While discharge capacities of 665.6, 572.7, 522.4 and 448.6 mAh g^{-1} at the same current densities are obtained in $NaClO_4$-EC/PC. The good reversibility, rate capability and cyclic performance of electrodes in $NaCF_3SO_3$-DGM is similar to results reported for Na/FeS_2 system in the literature [11-12], in which the ether-based electrolyte was believed to suppresses the reactions between possible sodium polysulfide and electrolyte. After 50 cycles at different current densities, the CoS_2/MWCNT electrodes remain reversible capacities of 679 and 548 mAh g^{-1} in $NaCF_3SO_3$-DGM and $NaClO_4$-EC/PC electrolytes respectively, while the values of CoS_2 electrodes are only 414 and 200 mAh g^{-1} respectively.

In order to reveal the origin of the better electrochemical performance of CoS_2/MWCNT electrodes, the *ex situ* TEM and SAED techniques are utilized to examine their compositions and structures of the discharged and charged products. Fig. 3(a-f) shows TEM images and corresponding SAED patterns of CoS_2/MWCNT electrodes after the firstly discharged to 1.0 V, respectively. The data of CoS_2 are included for comparison. The similar particles of the sodiated products as the initial (Fig. 1(c) are observed with the average size of 200 nm (Fig. 3(a)). The enlarged TEM image of a fully sodiated CoS_2 particle as shown in Fig.3 (b) shows that the nanograins with sizes about 5 nm are uniformly distributed in the matrix phase. The corresponding SAED pattern in this area is shown in Fig. 3(c) and all diffraction rings can be perfectly indexed as a mixture of Na_2S (JCPDS No. 23-0441) and Co (JCPDS No. 15-0806). As shown in Fig. S5 (a), the typical nanograins with the fringe spacing of 0.20 nm and 0.33 nm can be well indexed as the (111) planes of Co and the (111) planes of Na_2S, respectively. As a result, nanograins in the enlarged TEM image can be assigned to Co grains (marked by red circles) and the matrix can be indexed to Na_2S phase (marked by black arrow). It is interesting to find that TEM images of bare CoS_2 electrodes after the discharged to 1.0 V (Fig. 3(d)) are utterly different from those of CoS_2/MWCNT electrodes, and heavily particles aggregation of the sodiated products can be observed after the bare CoS_2 electrode is discharged. As shown in the enlarged TEM image (Fig. 3(e)), aggregation of sodiated products seems to result in cracking of the particles, which may be responsible for the poor electrochemical performance of bare CoS_2 electrodes. The main components of the discharge product are also confirmed to be Co and Na_2S phases by SAED (Fig. 3(f)) and HRTEM results (Fig. S5 (b)). According to the TEM results described above, the evolution processes of CoS_2/MWCNT and

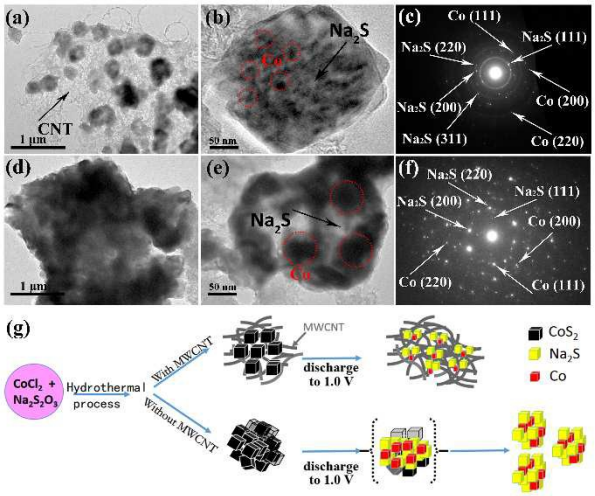

Figure.3 *Ex situ* TEM images and corresponding SAED patterns of sodiated electrodes (a-c) CoS_2/MWCNT and (d-f) bare CoS_2. (g) Schematic diagram for the evolution process of the as-prepared CoS_2/MWCNT and bare CoS_2 electrodes before and after the first discharged to 1.0 V.

bare CoS_2 electrodes before and after the first discharged to 1.0 V are illustrated in Fig. 3(g). For CoS_2/MWCNT electrodes, CoS_2 nanoparticles are uniformly dispersed on the MWCNT as shown in Fig. 1(c). Apparently, the sizes of CoS_2 nanoparticles in CoS_2/MWCNT electrodes are smaller than those in the bare CoS_2 electrodes (Fig. 1(e)), and MWCNT could efficiently prevent CoS_2 nanoparticles from aggregation. After two electrodes of CoS_2/MWCNT and bare CoS_2 are discharged to 1.0 V, the composition of two electrodes change from CoS_2 into metal Co and Na_2S. Because of both strength and flexibility of MWCNT, active particle separation or aggregation can be obviated during the discharge process. CoS_2/MWCNT could ensure nanosized metal Co uniformly distributed in Na_2S matrix after the discharged to 1.0 V, which is quite unlike bare CoS_2 electrodes.

When CoS_2/MWCNT electrodes are charged to 2.9 V, the nanoparticles with the size of 200 nm are dispersed randomly on the MWCNT network and almost same as the initial states, indicating the good reversibility of electrodes (Figure S6 (a)). The SAED pattern in this region is shown in Figure S6 (b). All d-spacing derived from SAED spectra can be well indexed to cubic CoS_2 (JCPDS No. 41-1471). The existence of CoS_2 after charging to 2.9 V provides direct evidence to conversion reaction of Co and Na_2S into CoS_2, which can be further supported by XAFS results shown in Fig. S7. The electrochemical reaction mechanisms of both CoS_2/MWCNT and CoS_2 electrodes with sodium are the same, and can be expressed as

$CoS_2 + 4Na + 4e^- \longleftrightarrow Co + 2Na_2S$ (1),

but, their electrochemical performances are quite different. CoS_2/MWCNT electrode could deliver the discharge capacity of 568 mAh g^{-1} in $NaCF_3SO_3$-DGM after 100 cycles while only the discharge capacity of 190 mAh g^{-1} after 100 cycles is preserved for the CoS_2 electrode in $NaCF_3SO_3$-DGM. Two discharge reactions of CoS_2/MWCNT and CoS_2 electrodes with sodium generate the same discharge products of Co and Na_2S (Equ. (1)). Interestingly, it can be found that the nanosized metal Co is highly dispersed in the Na_2S matrix as shown in Fig. 3(a) in sodiated CoS_2/MWCNT electrodes. However, metal Co is aggregated as shown in Fig. 3(e) in sodiated CoS_2 electrodes. It is the difference of nanosized metal Co uniformly distribution in Na_2S matrix formed after the discharge process that should be responsible for the better cycling performance of CoS_2/MWCNT electrodes than that of CoS_2 electrodes. Similarly recent reports using CNT additives in the composite electrodes improving the cycling behavior with CNTs over other carbon additives in lithium ion batteries[27-28], MWCNT hold three dimensional electron conductive networks with high surface area, which facilitates the fast penetration of sodium ions and diffusion of electrolytes. In addition, MWCNT may be used as an elastic buffer that prevents breaking up of electrode while keeping intact the structural integrity of active nanoparticles. These advantages for using MWCNTs in sodium ion batteries as an additive within composite electrodes should play important role in increasing the reversible capacity, enhancing the rate capability, and improving cyclability.

Conclusion

CoS_2/MWCNT nanocomposites are synthesized by a simply hydrothermal process and the MWCNT plays an important role for excellent electrochemical performance of CoS_2/MWCNT electrodes. Besides, the electrochemical performance of CoS_2/MWCNT electrodes in $NaCF_3SO_3$-DGM is better than that in $NaClO_4$-EC/PC electrolyte, indicating that $NaCF_3SO_3$-DGM electrolyte is well choice for Na/CoS_2 system. Furthermore, the huge energy density of 1027 Wh kg^{-1} is obtained for CoS_2/MWCNT electrode, which is the highest value among all metal-based electrodes previously reported. Our results have demonstrated that integration of CoS_2 with MWCNT and optimization of electrolyte are beneficial for the reversibility of CoS_2 electrode, thereby offering fundamental concepts to rationally design metal sulfides with higher performance for SIBs.

This work was financially supported by the NSAF (Grant No.U1430104), 973 Program (No.2011CB933300) of China, Science & Technology Commission of Shanghai Municipality (08DZ2270500 and 11JC1400500), and National Foundation of China (No.B1120132029)

Notes and references

† Electronic Supplementary Information (ESI) available: experimental details, discharge/charge curves of electrodes in $NaClO_4$-EC/PC electrolyte, CV curves, TEM and SAED patterns of electrodes after charging to 2.9 V, Co K-edge XANES spectra. See DOI:

[1]P. Veronica, S. Paula, V. Irune, B. H. Karina, C. G. Javier, R. Teofilo, *Energy Environ. Sci.* 2012, *5*, 5884-5901.
[2]D.S. Michael, D. H. Kim, L. Eungje, S. J. Christopher, *Adv. Func. Mater.* 2013, *23*, 947-958.
[3] H. L. Pan, Y. S. Hu, L.Q. Chen, *Energy Environ. Sci.* 2013, *6*, 2338–2360.
[4]H. S. Ryu, J.S. Kim, J. S. Park, J. W. Park, K. W. Kim, J. H. Ahn, T. H. Nam, G. Wang, H. J. Ahn, *J. Electrochem. Soc.* 2013, *160(2)*, 338-343.
[5]K. D Prasit, K. S Uttam, M. Sagar, *RSC Adv.* 2014, *4*, 43155–43159.
[6]J. S. Kim, D. Y. Kim, G. B. Cho, T. H. Nam, K. W. Kim, H. S. Ryua, J. H. Ahn, *J. Power Sources* 2009, *189*, 864–868.
[7]J. S. Kim, S. W. Lee, X. J. Liu, G. B. Cho, K. W. Kim, I. S. Ahn, J. H. Ahn, G. X. Wang, H. J. Ahn, *Curr. Appl. Phys.* 2011, *11*, 11-14.
[8]Y. X. Wang, K. H. Seng, S. L. Chou, J. Z. Wang, Z. P. Guo, D. Wexler, H. K. Liu, S. X. Dou, *Chem. Commun.* **2014**, *50*, 10730-10733.
[9]D. W. Su, S. X. Dou, G. X. Wang, *Chem. Commun.* 2014, *50*, 4192—4195.
[10]A. Kitajou, J. Yamaguchi, S. Hara, S. Okada, *J. Power Sources* 2014, *247*, 391-395
[11]Y. J. Zhu, L. M. Suo, T. Gao, X. L. Fan, F. D. Han, C. S. Wang, *Electrochem. Commun*. 2015**,** (DOI: 10.1016)
[12]Z. Hu, Z. Q. Zhu, F. Y. Cheng, K. Zhang, J. B. Wang, C. C. Chen, J. Chen, *Energy Environ. Sci.* 2015, (DOI: 10.1039)
[13]Y. M. Xiao, J. H. Wu, J. Y. Lin, S. Y. Tai, G. T. Yue, *J. Mater. Chem. A* 2013, *1*, 1289–1295.
[14]E. B. Bi, H. Chen, X. D. Yang, W. Q. Peng, G. Michael, L. Y. Han, *Energy Environ. Sci.* 2014, *7*, 2637–2641.
[15]S. F. Matthew, K. Park, C. A. Miguel, K. S Pralay, S. Jin, *J. Phys. Chem. Lett.* 2013, *4*, 1843−1849.
[16]Y. Ji, X. Y. Liu, W. Liu, Y. Wang, H. D. Zhang, M. Yang, X. F. Wang, X. D. Zhao, S. H. Feng, *RSC Adv.* 2014, *4*, 50220–50225.
[17]J. C. Xing, Y. L. Zhu, Q. W. Zhou, X. D. Zheng, Q. J. Jiao, *Electrochim. Acta* 2014, *136*, 550–556.
[18]S. J. Peng, L. L. Li, H. T. Tan, R. Cai, W. H. Shi, C. C. Li, G. M. Subodh, S. Madhavi, R. Seeram, Q. Y. Yan, *Funct. Mater.* 2014, *24*, 2155–2162.
[19]J. M. Yan, H. Z. Huang, J. Zhang, Z. J. Liu, Y. Yang, *J. Power Sources* 2005, *146*, 264–269.
[20]Q. M Su, J. Xie, J. Zhang, Y. J. Zhong, G. H. Du, B. S. Xu, *ACS Appl. Mate. Inter.* 2014, *6*, 3016-3022.
[21]G. C. Huang, T. Chen, Z. Wang, K. Chang, W. X. Chen, *J. Power Sources* 2013, *235*,122-128.
[22]Y. M. Wang, J. J. Wu, Y. F. Tang, X. J. Lu, C. Y. Yang, M. S. Qin, *ACS Appl. Mater. Interfaces* 2012, *4*, 4246−4250.
[23]Q. H. Wang, L. F. Jiao, Y. Han, H. M. Du, W. X Peng, Q. N. Huan, D. W. Song, Y. C. Si, Y. J. Wang, H. T. Yuan, *J. Phys. Chem. C* 2011, *115*, 8300–8304.
[24]J. Xie, S. Y. Liu, G. S. Cao, T. J. Zhu, X. B. Zhao, *Nano Energy* 2013, *2*, 49-56.
[25]B. Qiu, X. Y. Zhao, D. G. Xia, *J. Alloys Comp.* 2013, *579*,372–376.
[26]E Anastassakis, C. H Perry, *J. Chem. Phys.* 1976, *64*（9）, 3604-3609.
[27]Y. H. Yin, X. T. Zhang, Y. J. Jia, Z. X. Cao, S. T. Yang, *RSC Adv.* 2015*, 5,* 1447-1451.
[28]G. Gao, Q. Zhang, X. B. Cheng, P. Y. Qiu, R. J. Sun, T. Yin, D. X. Cui, *ACS Appl. Mater. Interfaces* 2015*, 7,* 340-350